



City Research Online

City, University of London Institutional Repository

Citation: Viphavakit, C., Komodromos, M., Themistos, C., Mohammed, W. S., Kalli, K. & Rahman, B. M. (2015). Optimization of a horizontal slot waveguide biosensor to detect DNA hybridization. *Applied Optics*, 54(15), pp. 4881-4888. doi: 10.1364/ao.54.004881

This is the accepted version of the paper.

This version of the publication may differ from the final published version.

Permanent repository link: <https://openaccess.city.ac.uk/id/eprint/12218/>

Link to published version: <https://doi.org/10.1364/ao.54.004881>

Copyright: City Research Online aims to make research outputs of City, University of London available to a wider audience. Copyright and Moral Rights remain with the author(s) and/or copyright holders. URLs from City Research Online may be freely distributed and linked to.

Reuse: Copies of full items can be used for personal research or study, educational, or not-for-profit purposes without prior permission or charge. Provided that the authors, title and full bibliographic details are credited, a hyperlink and/or URL is given for the original metadata page and the content is not changed in any way.

City Research Online:

<http://openaccess.city.ac.uk/>

publications@city.ac.uk

Optimization of a horizontal slot waveguide biosensor to detect DNA hybridization

Charusluk Viphavakit,^{1*} Michael Komodromos,¹ Christos Themistos,¹ Waleed S. Mohammed,² Kyriacos Kalli³, and B.M.Azizur Rahman⁴

¹Department of Electrical Engineering, Frederick University, 7 Frederickou Str., Nicosia, 1036, Cyprus

²Center of Research in Optoelectronics, Communication and Control System (BU-CROCCS), Bangkok University, Paholyotin Rd., Klong Luang, 10120, Pathumthani, Thailand

³Department of Electrical Engineering, Cyprus University of Technology, Limassol 3036, Cyprus

⁴Department of Electrical Engineering, City University London, Northampton Square, London EC1V 0HB, UK

*Corresponding author: charusluk.v@gmail.com

Received Month X, XXXX; revised Month X, XXXX; accepted Month X, XXXX; posted Month X, XXXX (Doc. ID XXXXX); published Month X, XXXX

A full-vectorial **H**-field formulation-based finite element approach is used to optimize a biosensor structure incorporating a horizontal slot waveguide. It is designed to detect DNA hybridization through the change of the effective index of the waveguide structure. The key parameters, such as normalized power confinement, power density, change in effective index and sensitivity are presented by optimizing the device parameters of the slot waveguide. It is shown here that a 90.0 μm long compact Mach-Zehnder section can be designed with horizontal slot waveguide to detect DNA hybridization and for a ring resonator arrangement a sensitivity of 893.5 nm/RIU is obtained.

OCIS codes: (050.6624) Subwavelength structures; (130.6010) Sensors; (230.7400) Waveguides, slab; (280.4788) Optical sensing and sensors.
<http://dx.doi.org/10.1364/AO.99.099999>

1. Introduction

Optical sensors have been studied extensively in the past few decades since they can be used in many application areas such as environmental monitoring to detect the heavy ions in the water [1], quality control and process monitoring in the food industry [2], and medical diagnostics [3-5]. There are two categories of biosensors based on the detection technique, namely fluorescence-based sensors [6, 7] and label-free sensors [8, 9]. Fluorescence based biosensors are very sensitive and can be scaled down to single-molecule detection [10] but fluorescence-tag formation through covalent bonds between molecules and fluorophores is required in the detection process. However, the ability of fluorophores to fluoresce during the light excitation is reduced due to the accumulation of chemical damage from excited electrons known as photobleaching [7]. Label-free biosensors eliminate the need for the tags allowing real time detection. The use of biological molecules in natural form avoids the need of using the tags. Biosensors involving nucleic acid are also known as genosensors which is based on the base pairing of complementary DNA or the hybridization process. The interaction between single-stranded DNA-probe (ssDNA) with the target-probe can generate the optical signal [11-13].

The silicon-on-insulator (SOI) based nanowires have been widely used as the label-free biosensor to detect the change of optical signal from the hybridization process [14, 15]. The SOI technology has been attractive for its high index contrast and low

optical power losses [16-18]. The silicon nanowire optical sensors detect the change of effective index from the light confined in the guiding area which occurs either due to the change of the refractive index of the cladding medium, known as homogeneous sensing, or exploiting the change of a thin layer structure on the waveguide surface called surface sensing [17]. Conventionally the light is guided in a higher refractive index area of the waveguide, which is mostly sandwiched by the SOI substrate and the cladding material, such as air or water. Therefore, the light interaction with the sensing material in the cladding region or at the surface of the waveguide is limited, leading to the low sensitivity of the device. Recently, a novel concept has been reported where light can be confined in a low-index region and thus allowing easy access to high field region. The enhancement of light interaction in the sensing region for sensitivity improvement makes the SOI silicon slot waveguide technology a growing field of interest [19-21]. The slot waveguide is fabricated in a way to have two higher refractive index nanowires close to each other. The narrow gap between those two nanowires has a lower refractive index. For the slot waveguide, the light is confined in the lower refractive index area due to the discontinuity of the normal component (E_n) of the electric field (**E**-field) at the interface. As a consequence, a large fraction of the light energy can be confined in the slot region and this fraction can be influenced by the presence of the sensing medium to yield a highly sensitive sensor.

There are two possible types of slot waveguides, relating to their structure orientations, namely the vertical and horizontal slot waveguides. Both the quasi-TE and quasi-TM modes can be supported by the vertical and horizontal slot guides. However, for the vertical slot only the quasi-TE mode confines better in the slot region, and similarly only the quasi-TM mode for the horizontal slot. Recently, research work on the use of the vertical slot waveguide to use as biosensors [22] and also to detect the DNA-hybridization has been proposed in [9, 23]. The sensitivity of silicon nitride vertical slot waveguide integrated with Mach-Zehnder interferometer (MZI) can be $1864\pi/\text{RIU}$ (refractive index unit) [23]. Also, the sensitivity of vertical multiple-slot waveguides has been found to be three times better than the single slot waveguide [22]. However, there is a limitation in the fabrication process involving etching of the vertical narrow gap. Surface roughness can occur during the etching process due to the sub-micron size dimension, leading to increased scattering loss[24]. For the horizontal slot waveguide, the structure can be fabricated using the chemical vapor deposition (CVD) and thermal oxidization techniques. These techniques can be applied layer by layer and result in a smoother surface and consequently reduced scattering loss [25, 26].

In this work, the DNA-hybridization process where the ssDNA is base-paired with another ssDNA to form double-stranded DNA (dsDNA) is studied by using a horizontal slot. The dimensions of the horizontal structure have been optimized to obtain the maximum optical field intensity in the sensing region, using a full-vectorial Finite Element Method (FEM) [27]. The propagation constant, effective index, normalized power confinement and power density of the fundamental quasi-TM mode of the device have been investigated by using this approach. In this paper, the material sample assumed to be sensed is taken as DNA. Change in the effective index when a single-stranded DNA becomes double-stranded DNA is calculated, and sensitivity of this device is discussed.

2. Numerical Calculations

The Finite Element Method (FEM) has been established as one of the most powerful numerical techniques, because of its accuracy, flexibility and versatility in the numerical analysis of optical waveguides, particularly in structures with arbitrary shapes, index profiles, nonlinearities and anisotropies. In the present work a full-vectorial \mathbf{H} -field finite element formulation has been applied for the modal analysis of the quasi-TM mode in the horizontal slot nanowire structure to determine the propagation characteristics of the fundamental optical mode. The governing eigenvalue equation can be generated by minimizing the variational energy functional given below [27]:

$$\omega^2 = \frac{\int [(\nabla \times \mathbf{H})^* \cdot \epsilon^{-1} (\nabla \times \mathbf{H}) + p(\nabla \cdot \mathbf{H})^* (\nabla \cdot \mathbf{H})] dx dy}{\int \mathbf{H}^* \cdot \mu \mathbf{H} dx dy} \quad (1)$$

where \mathbf{H} is the full-vectorial magnetic field, * represents a complex conjugate and transpose, ω is angular frequency of the wave, ω^2 is the eigenvalue, and ϵ and μ are the permittivity and permeability, respectively.

In this paper, the fabrication parameters of the horizontal slot waveguide including the structure width, the core height, and the slot height are optimized for sensing applications, using this \mathbf{H} field formulation. The \mathbf{E} field and the energy flux density represented by Poynting vector (\mathbf{S}) have also been calculated.

3. Results and Discussion

The horizontal slot waveguide can be fabricated on an SOI substrate, where a low-index layer (slot) is sandwiched by two high-index poly-silicon layers. Most of the horizontal slots consist of low-index solid material in the slot region. However, it is also possible to fabricate similar slot waveguide with gas or liquid in the slot region. In this work, the horizontal slot waveguide is designed to be connected with the tapered waveguide and feed waveguide as shown in Fig. 1. The nanowire is fabricated layer-by-layer starting from poly-silicon followed by SiO_2 , and then poly-silicon again. Following that, the oxide layer can be etched away using Buffered Oxide Etch (BOE). The oxide layer at the nanowire region will be removed first due to its smallest width leaving an air-gap between the two poly-silicon layers. Once the low-index oxide layer under the narrow waveguide region is removed then the etching process is stopped so that the two silicon layers are mechanically supported by the wider region at the two ends where silica was only partially removed. The slot height depends on the thickness of the oxide layer which can be better controlled during the dry oxidation process. The tapered waveguide and feed waveguide not only support the nanowires physically, but also reduces the insertion loss when connecting nanowire to a light source or other optical devices.

The horizontal slot waveguide is proposed to be used in bio-sensing applications, such as for DNA hybridization. The sensor is designed to detect the change of effective index when the sensing material has the refractive index change. In this case, the sensing materials have to be bonded with the thin layers inside the slot region, which are called linkers. They act as a glue in order to form a selective physical or chemical bonding with the sensing materials. A cross section of the horizontal slot waveguide with the sensitive layer proposed in this paper for the numerical simulations is also shown in Fig. 1.

As mentioned above, the horizontal slot waveguide is investigated as a possible sensor to detect DNA hybridization. The DNA hybridization is the process of combining two ssDNA to become dsDNA. The ssDNA and dsDNA have different refractive indices which are taken as 1.456 and 1.53 [28], respectively. With the change of refractive index in ssDNA and dsDNA, the effective index of the whole structure is also changed. The thicknesses of the ssDNA and dsDNA layers are fixed to be 8 nm for the initial study. The refractive index of the poly-silicon core layers is 3.9. In

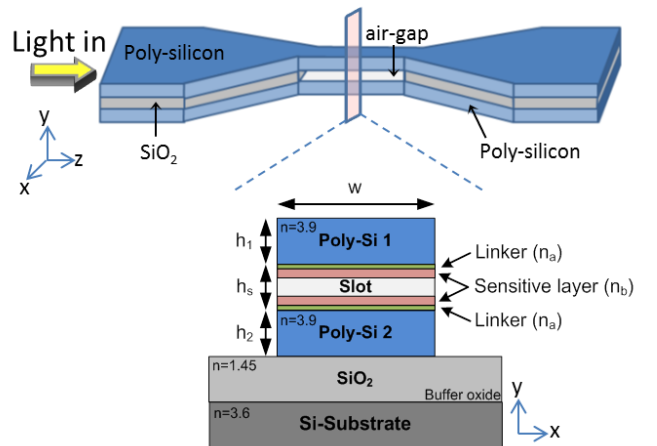


Fig 1. A schematic of the horizontal slot waveguide for the simulation analysis to detect the DNA hybridization in 3D (Top) and its cross section (Bottom).

the simulation, the slot area is assumed to be filled with water, this is the same as the cladding material since it is the main constituent material of the stock solution [29], which has a refractive index value of 1.33. To immobilize the ssDNA, silanes with the refractive index of 1.42 (n_a) is used as the linker layer to form the covalent bond with the ssDNA, and it has a thickness of 1 nm. We have exploited the existing one-fold symmetry and used 34,000 first order triangles to represent only half of the structure. The main advantage of the FEM over the other numerical methods is that FEM can incorporate triangles of different shapes and sizes to obtain the numerical efficiency. In

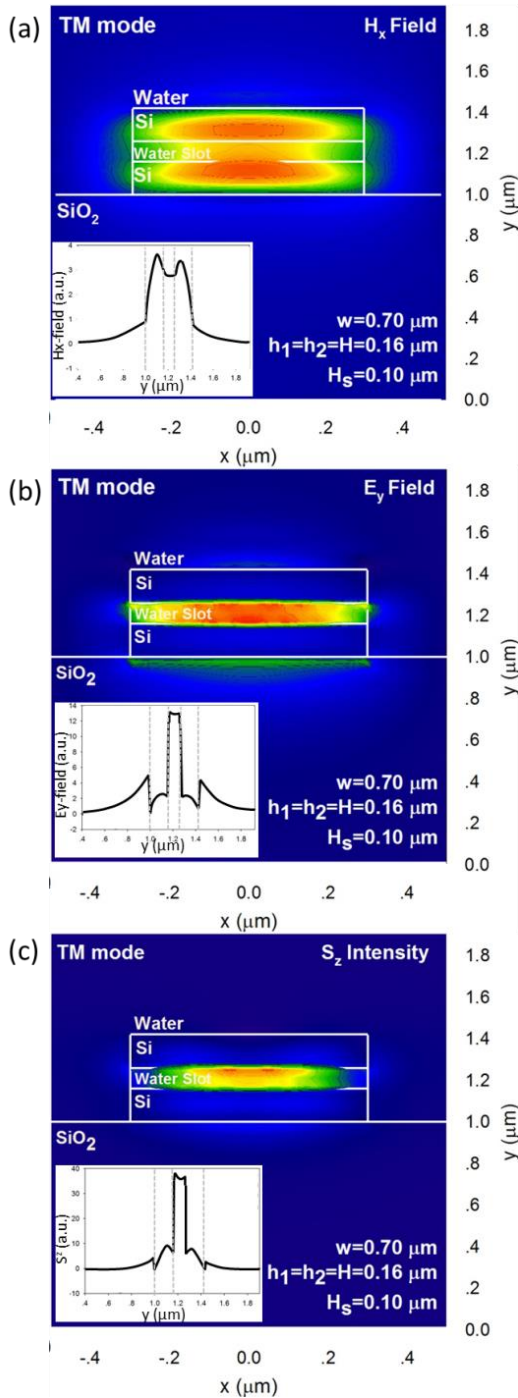


Fig 2. A contour plot of (a) H_x field, (b) E_y field, and (c) Energy flux density Poynting vector: S_z^2 . Insets are the field plots along the y-axis.

this case to represent the 1 nm thick linker layer, vertical resolutions used here was 0.2 nm or better. The key parameters that needs to be optimized are the width (w) of the structure, the poly-silicon core heights (h_1 and h_2), and the slot height (h_s). The operating wavelength in this work is taken at 1550 nm.

In the modal solution using the FEM approach the existing half symmetry has been considered for the horizontal slot waveguide. The quasi-TM mode, where the dominant electric field is normal to the interface, is considered because it has a higher confinement in the slot region compared to the quasi-TE mode. For the quasi-TM mode, the H_x field is the dominant component of the \mathbf{H} -field. The contour of the dominant H_x field of the waveguide for a width (w) of 0.70 μm , poly-silicon core height (h_1, h_2) of 0.16 μm and a slot height (h_s) of 0.10 μm is shown in Fig. 2(a). The H_x field has a maximum intensity in both the poly-silicon core layers. However, the maximum intensity is not at the center of the core region but it is closer to the interface between the core region and the slot area, as it can be seen in the inset of Fig. 2(a), showing H_x profile in y-direction.at the center the waveguide

The fundamental E_y field has also been derived from the \mathbf{H} -field and shown in Fig. 2(b) and its inset. The E_y field along the y-direction given as an inset shows the discontinuity at the interface of core and slot regions providing the strong field in the slot area. The energy flux density or so called Poynting vector (S^2) presented in Fig. 2(c) which has been calculated from the \mathbf{E} and \mathbf{H} fields. It can be clearly seen that the energy is more confined in the slot area, thus confirming the light is guided in the low-index region of the slot waveguide.

3.1 The effect of poly-silicon core height (H)

The effect of the variations of the poly-silicon core height, H , which is considered to be symmetric ($h_1=h_2=H$) has initially been examined, where the width, w , and the slot height, h_s , were assumed to be fixed at 0.7 μm 0.10 μm , respectively. The normalized power confinement and the power density in the sensing layer (DNA probe) with the variations of the core height are presented in Fig. 3. The dimension-less normalized power confinement is the power in that region normalized with the total power. The power density is obtained by dividing this normalized power confinement with the area of that region. The total normalized power confinement in the sensing area, as shown in Fig. 3 is the sum of the normalized power confinement in the upper and lower DNA probe layers, each having a thickness of 8

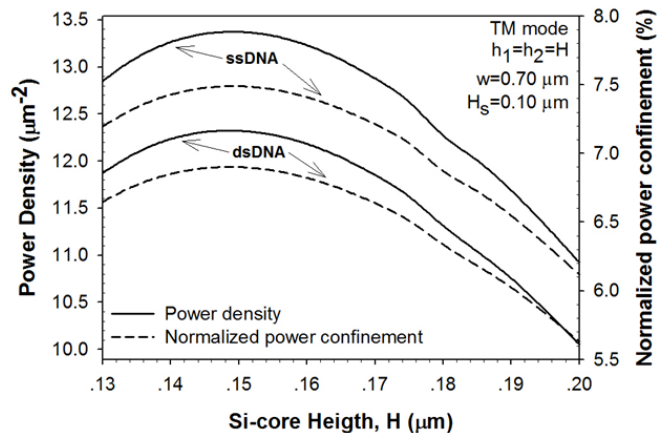


Fig. 3. Variations of power density and power confinement in the sensing layer (DNA probe) with the core height, H .

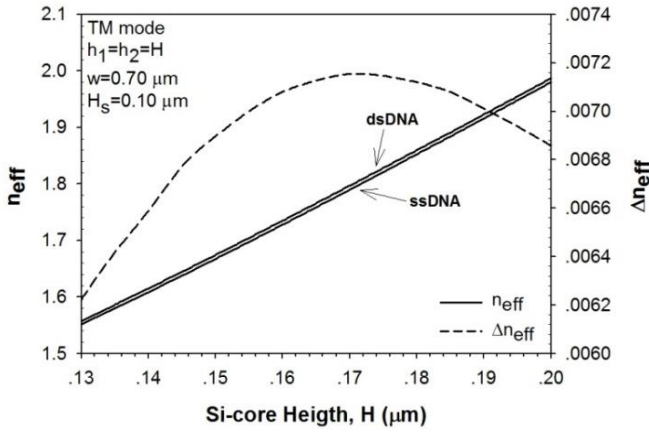


Fig. 4. Variations of the effective index difference and the effective index in each sensing material with the core height.

nm. The power density is the average power density for both DNA probe layers. The normalized power confinement and power density exhibit a similar trend when the core height is varied as the sensing area size does not change when H is varied. At a smaller core height, both the normalized power confinement and the power density in the sensing layers are initially low because the structure gets close to the cut-off limit. Therefore, the optical power reduction occurs due to an evanescent wave spreading into the cladding medium and the buffer oxide layer. Then the power increases with the core height, due to the enlargement of the guided area, until reaching a maximum confinement at a height, H of $0.15 \mu\text{m}$. However, if the core height is too large, the light will mainly be guided only inside the poly-silicon core region. Consequently, the normalized power confinement and power density in sensing region are decreased as the core height increases further. It is also shown that the ssDNA ($n_b=1.456$) has higher power in the sensing medium compared to the dsDNA ($n_b=1.530$). This is due to the higher refractive index contrast in ssDNA compared to dsDNA which leads to the larger discontinuity in the electric field. If the whole slot region is used for a particular device operation, such as polymer filled electro-optic modulator, then normalized power confinement is the key design parameter. However, if a sensing material is localized only at the interfaces then the power density around that region will be a more important parameter.

One of the most important parameters in biosensing applications is the change of effective index which can be used to calculate the sensitivity of the device. In a Mach-Zehnder arrangement, the change in effective index will yield a phase change between the branches. Variations of the effective index with the core height is shown in Fig. 4, where the effective index due to presence of each sensing material is included. Due to a smaller refractive index value of ssDNA, we found out that $n_{\text{eff,ssDNA}} < n_{\text{eff,dsDNA}}$. However, the effective index increases when the poly-silicon core height is increased for both ssDNA and dsDNA because of the larger silicon volume. The change in effective index, shown by a dashed line, increases when the core height is increased until it reached a maximum value at a height of $0.17 \mu\text{m}$. At a height greater than $0.17 \mu\text{m}$, the structure becomes too large, and light is mostly confined in the core rather than in the slot. This leads to a reduction of the change of effective index as well as the sensitivity of the waveguide.

3.2 The effect of structure width (w)

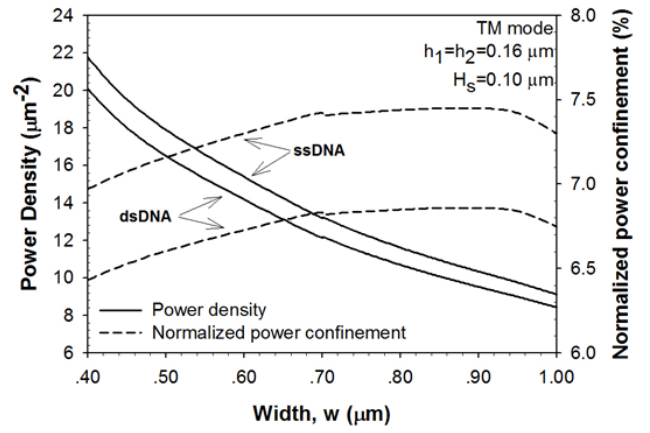


Fig. 5. Variations of the power density and power confinement in the sensing layer (DNA probe) with the width.

It was shown in Fig. 3 that the maximum power density was achieved when $H \sim 0.15 \mu\text{m}$. On the other hand, Fig.4 indicates that maximum n_{eff} can be obtained when $H \sim 0.17 \mu\text{m}$. Although their variations were rather small in this region, so for subsequent optimization, we have considered $H = 0.16 \mu\text{m}$. The thickness of the linker layer (silanes) and the sensing medium (DNA) remained the same at 1 nm and 8 nm , respectively. Next, the normalized power confinement and power density with the variations of the width of the waveguide are simulated and presented in Fig. 5. At smaller width, the normalized power confinement in the slot region is less due to the smaller size of the structure, where the mode approaches cut-off. Therefore, only some light is guided in the guiding region, and the rest is spread into the cladding region. When the width is increased, the normalized power confinement is also slightly increased. In the case of the ssDNA ($n_b=1.456$), the normalized power confinement is higher than that of the dsDNA ($n_b=1.530$), due to the higher refractive index contrast. On the other hand, the power density is inversely proportional to the width. At smaller width, the power density is high because the guiding area is smaller. As the width increases, the power per unit area is reduced due to the larger guiding area. However, higher power density is observed in the ssDNA than in the dsDNA due to higher normalized power confinement.

Earlier results from above have shown that the change of the core height is more significant to the normalized power confinement than the change of the width. Next, the variations of

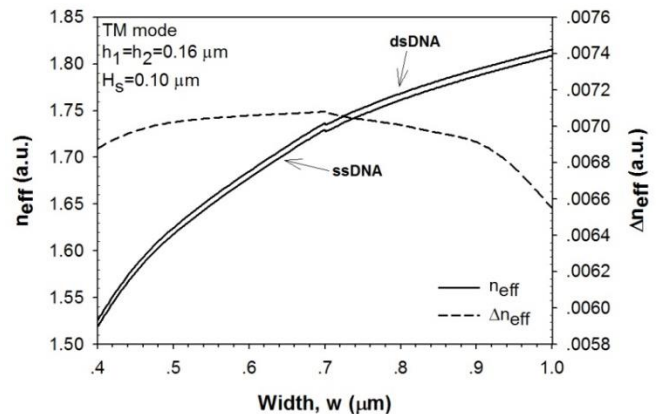


Fig.6. Variations of the effective index difference and the effective index in each sensing material with the width.

effective index and the effective index difference due to the presence of each sensing layer with respect to the structure width are examined and presented in Fig. 6.

The effective index due to the presence of each sensing layer, represented by two solid lines, increase with the increasing width of the structure because the light can be more confined in the larger structure. In addition, $n_{\text{eff,dsDNA}} > n_{\text{eff,ssDNA}}$ because dsDNA has larger refractive index. The effective index change is gradually affected with the structure width. The change in the effective index, shown by a dashed line, is slightly increased when the width increases up to $0.7 \mu\text{m}$. When the width is larger than $0.7 \mu\text{m}$, the change of effective is continuously decreased. Comparing these with the previous results shown above, the change of effective index is affected more by the core height rather than the width as the graph changes more rapidly when varying the core height.

3.3 The effect of slot height (h_s)

The next variable in this study is the slot height (h_s). The normalized power confinement and the change of effective index are demonstrated with various values of slot height as shown in Fig. 7.

The slot structure has a fixed core height and width with values $0.16 \mu\text{m}$ and $0.70 \mu\text{m}$, respectively. The normalized power confinements in the ssDNA and dsDNA layers, shown by two solid lines, exhibit a similar trend. Their normalized power confinement is reduced when the slot height is increased. At a larger slot height, the separation gap between the two poly-silicon core layers is larger. Thus, the power is coupled more into the poly-silicon core instead of the slot, leading to a reduction of the normalized power confinement in the slot area. As the ssDNA has greater refractive index contrast than the dsDNA, it also has higher normalized power confinement. In addition, the effective index difference represented by a dashed line decreases with increasing slot height.

Even though a smaller slot height provides a larger effective index difference, it would be difficult to create a very small and uniform slot due to the fabrication limits. However, the slot height of $0.10 \mu\text{m}$ is selected in this work because it is the minimum value which is suitable for the biosensing application. Next, the change of effective index with various values of slot height is studies again with different slot height and structure width in order to obtain the best possible results for the design. The relation of the effective index change with the slot height at

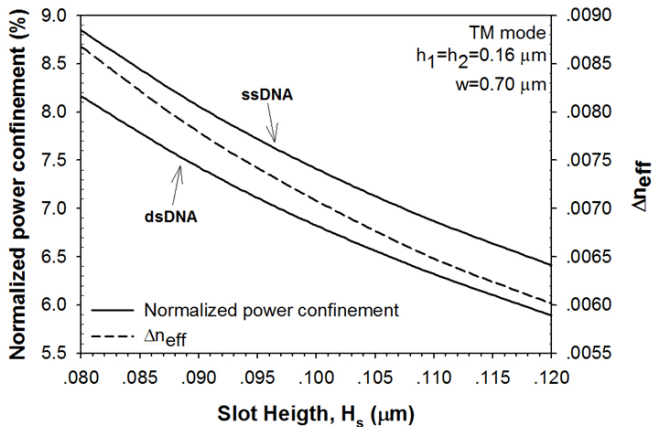


Fig. 7. Variations of the effective index difference and the power confinements with the slot height.

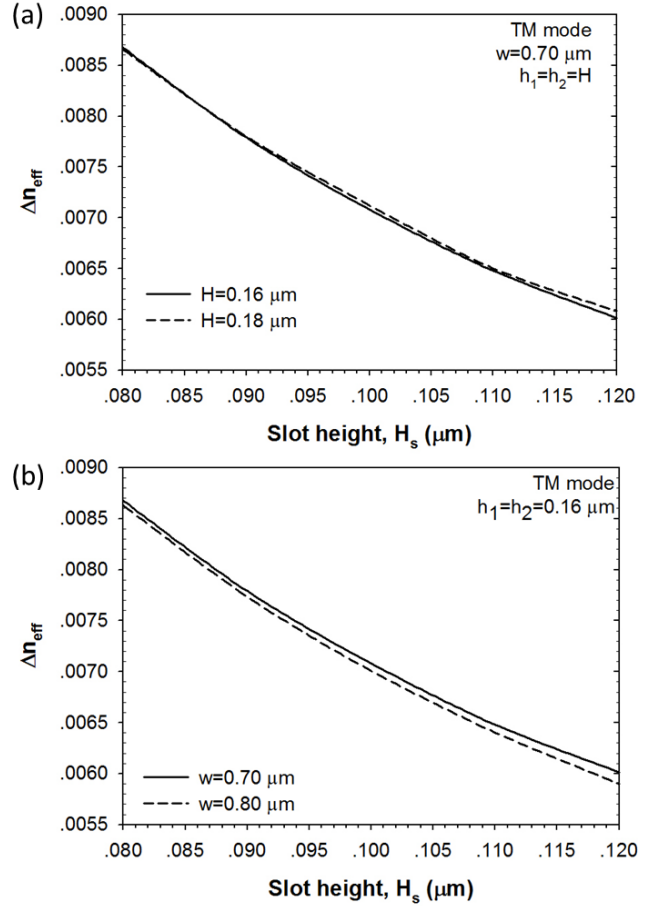


Fig.8. Variations of the effective index difference with the slot height at different (a) core heights and (b) core width.

different core heights and different widths are calculated and shown in Figs. 8(a) and 8(b), respectively. Fig. 8(a), the change of effective index has almost the same value when varying the slot height at the structure width of $0.7 \mu\text{m}$. For Fig. 8(b) shows the comparison between the structure with width of $0.70 \mu\text{m}$ and $0.80 \mu\text{m}$ at the fixed core height of $0.16 \mu\text{m}$. The smaller structure width represented in solid line has higher change of effective index when the slot height is varied.

In order to detect the DNA hybridization, this horizontal slot waveguide can be incorporated in a Mach-Zehnder Interferometer (MZI) system. By introducing the sensing slot waveguide in one arm of the MZI, the relative phase shift ($\Delta\phi$) can be obtained from the change in the effective index, Δn_{eff} as:

$$\Delta\phi = \Delta n_{\text{eff}} * \frac{2\pi}{\lambda} * L \quad (2)$$

The destructive interference or the minimum interference signal occurs when the phase difference is equal to π . Therefore, the length of the MZI arm (L) with horizontal slot waveguide needs to be $90.0 \mu\text{m}$ long when the slot height, $H_s = 80 \text{ nm}$ as shown in Fig. 8, when the maximum Δn_{eff} is achieved.

3.4 The sensitivity (S)

Since the horizontal slot waveguide is proposed for use in a biosensing application the sensitivity is a very important parameter for this waveguide. The sensitivity or Figure-of-Merit (FOM) of a biosensors can be defined in terms of the changes in intensity [30], or wavelength shift [9, 31] or effective index with

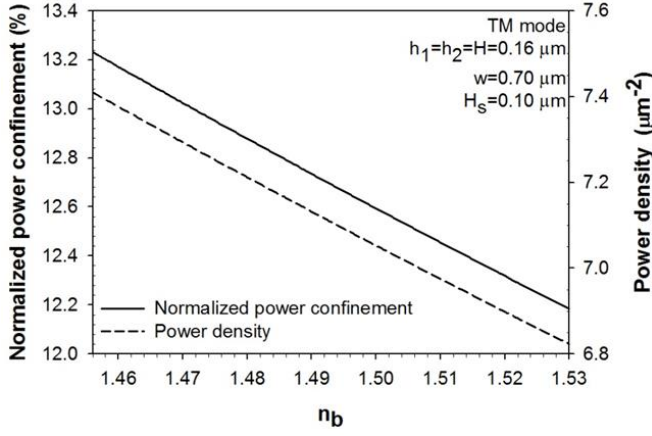


Fig. 9. Variation of the normalized power confinement and power density with the change in refractive index of the sensing material.

the background refractive index change [32] or other measurable parameters. For MZI based system, change in effective index, Δn_{eff} is directly related to the intensity profile, which in turn depends on the normalized power confinement and power density. Variations of the normalized power confinement and power density with the background cladding refractive index (which changes with the presence of the sensing materials) are shown in Fig. 9. It can be observed that the both power confinement and power density decreases when the cladding index is increased. This is due to smaller refractive index contrast between the waveguide and the slot region reducing the field enhancement there. Consequently, the sensitivity of the horizontal slot waveguide is reduced.

The horizontal slot waveguide sensitivity (S_{wg}) can be calculated using the following equations [33].

$$\Delta n = \frac{n_b - n_{b,ref}}{n_{b,ref}} \quad (3)$$

$$\Delta n_{eff} = \frac{n_{eff} - n_{eff,ref}}{n_{eff,ref}} \quad (4)$$

$$S_{wg} = \frac{\Delta n_{eff}}{\Delta n} \quad (5)$$

where n_b is the refractive index of sensing material, which in this case is either ssDNA or dsDNA, $n_{b,ref}$ is the reference refractive index which is kept fixed at 1.456 (ssDNA), n_{eff} is the effective index due to the presence of n_b , and $n_{e,ref}$ is n_{eff} at $n_{b,ref}$. The graph of sensitivity when changing the refractive index of the sensing material is shown in Fig. 10. This shows that the sensitivity is decreased when the refractive index of the sensing material is increased, similar as shown in Fig. 9. In this work, the horizontal waveguide is studied for detecting the DNA hybridization for example when ssDNA becomes dsDNA. Therefore, the sensitivity of the horizontal slot waveguide is reduced when ssDNA combines with complementary DNA and transforms into dsDNA. However, this hybridization process is reversible as the dsDNA can break down to become ssDNA again. For the reverse process, the sensitivity of the waveguide is enhanced.

The horizontal slot waveguide can also be incorporated in a ring resonator configuration to detect DNA hybridization. To compare the results with the previously reported work but using a vertical slot waveguide [9], the structural parameters of ring

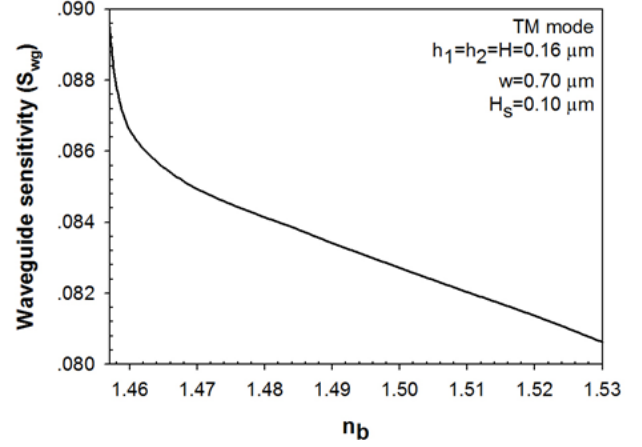


Fig. 10. The sensitivity of the horizontal slot waveguide with the variations of the refractive index of the sensing materials.

resonator are kept same but with a bending radius of 5 μm . The sensitivity of the device (S_{device}) can be calculated by using the equations below [9]:

$$S_{device} = \frac{\delta\lambda}{\delta n} \quad (6)$$

where, $\delta\lambda$ is the shift of resonance wavelength;

$$\delta\lambda = \frac{\delta n_{eff} * \delta\lambda_{res}}{n_g} \quad (7)$$

where δn_{eff} is the effective index difference when the hybridization occurs, $\delta\lambda_{res}$ is the resonance wavelength which is 1550 in this case, and n_g is the group index. The optimum horizontal slot waveguide structure proposed in this work has the width of 0.7 μm , the symmetric poly-silicon core height of 0.16 μm , and the slot height of 0.10 μm . With this structure, the sensitivity of 893.5 nm/RIU and the resonance wavelength shift of 6.33 nm are obtained. With the same waveguide material, the surrounding media, and the sensing material which is DNA, the sensitivity of the device incorporating horizontal slot waveguide is slightly higher compared to the vertical slot waveguide, where the sensitivity of 856 nm/RIU was reported [9]. The result presented here shows much improved sensitivity than that of 298 nm/RIU for a vertical slot on SOI [34] and 212 nm/RIU for a vertical slot waveguide using Si_3N_4 [35].

4. Conclusion

A full-vectorial **H**-field based finite element method has been used in the present work, for the study of a horizontal slot waveguide for biosensing applications. The above device was found to be sensitive with the variations of the refractive index difference in the sensing material. The sensing materials considered in the present work were ssDNA and dsDNA in the DNA hybridization process. The key parameters, such as normalized power confinement, power density, effective index difference, and sensitivity have been investigated and the fabrication parameters, such as the structure width, the core height, and the slot height have been optimized. The optimum dimensions for the slot waveguide structure, in order to achieve maximum normalized power confinement and large effective index difference, were found to be the following: width 0.7 μm , core height 0.16 μm and a slot height 0.10 μm and this yields a

compact design with the device length smaller than 100 μm . Furthermore, the sensitivity of this slot waveguide has been studied with the variations of the refractive index of the sensing material and for a ring resonator a significant improvement of the sensitivity value has been obtained. It has been shown that the sensitivity increases when the refractive index of the sensing material is reduced.

References

1. S. Haron and A. K. Ray, "Optical biodetection of cadmium and lead ions in water," *Medical Engineering & Physics* 28, 978-981 (2006).
2. L. D. Mello and L. T. Kubota, "Review of the use of biosensors as analytical tools in the food and drink industries," *Food Chemistry* 77, 237-256 (2002).
3. M. Marazuola and M. Moreno-Bondi, "Fiber-optic biosensors—an overview," *Analytical and Bioanalytical Chemistry* 372, 664-682 (2002).
4. E. Kress-Rogers, *Handbook of biosensors and electronic noses: medicine, food, and the environment* (CRC Press, 1996).
5. L. Heinemann and G. Schmelzeisen-Redeker, "Non-invasive continuous glucose monitoring in Type I diabetic patients with optical glucose sensors," *Diabetologia* 41, 848-854 (1998).
6. R. B. Thompson, *Fluorescence sensors and biosensors* (CRC Press, 2005).
7. W. G. Cox and V. L. Singer, "Fluorescent DNA hybridization probe preparation using amine modification and reactive dye coupling," *Biotechniques* 36, 114-123 (2004).
8. A. Star, E. Tu, J. Niemann, J.-C. P. Gabriel, C. S. Joiner, and C. Valcke, "Label-free detection of DNA hybridization using carbon nanotube network field-effect transistors," *Proceedings of the National Academy of Sciences of the United States of America* 103, 921-926 (2006).
9. T. Dar, J. Homola, B. M. A. Rahman, and M. Rajarajan, "Label-free slot-waveguide biosensor for the detection of DNA hybridization," *Appl. Opt.* 51, 8195-8202 (2012).
10. W. Moerner, "New directions in single-molecule imaging and analysis," *Proceedings of the National Academy of Sciences* 104, 12596-12602 (2007).
11. J. C. Pickup, F. Hussain, N. D. Evans, O. J. Rolinski, and D. J. Birch, "Fluorescence-based glucose sensors," *Biosensors and Bioelectronics* 20, 2555-2565 (2005).
12. T. Vo-Dinh and B. Cullum, "Biosensors and biochips: advances in biological and medical diagnostics," *Fresenius' journal of analytical chemistry* 366, 540-551 (2000).
13. A. Bonanni and M. Del Valle, "Use of nanomaterials for impedimetric DNA sensors: a review," *Analytica Chimica Acta* 678, 7-17 (2010).
14. Z. Gao, A. Agarwal, A. D. Trigg, N. Singh, C. Fang, C.-H. Tung, Y. Fan, K. D. Buddharaju, and J. Kong, "Silicon nanowire arrays for label-free detection of DNA," *Analytical Chemistry* 79, 3291-3297 (2007).
15. Y. L. Bunimovich, Y. S. Shin, W.-S. Yeo, M. Amori, G. Kwong, and J. R. Heath, "Quantitative real-time measurements of DNA hybridization with alkylated nonoxidized silicon nanowires in electrolyte solution," *Journal of the American Chemical Society* 128, 16323-16331 (2006).
16. D. M. Leung, X. Kan, B. M. A. Rahman, N. Kejalakshmy, and K. T. V. Grattan, "Optimizing the power confinement in silicon slot waveguides by use of Finite Element Method," in *SPIE/OSA/IEEE Asia Communications and Photonics* (International Society for Optics and Photonics, 2011), 83071A-83071A-83076.
17. F. Dell'Olivo and V. M. Passaro, "Optical sensing by optimized silicon slot waveguides," *Opt. Express* 15, 4977-4993 (2007).
18. A. Densmore, D.-X. Xu, P. Waldron, S. Janz, P. Cheben, J. Lapointe, A. Delage, B. Lamontagne, J. Schmid, and E. Post, "A silicon-on-insulator photonic wire based evanescent field sensor," *Photonics Technology Letters, IEEE* 18, 2520-2522 (2006).
19. V. R. Almeida, Q. Xu, C. A. Barrios, and M. Lipson, "Guiding and confining light in void nanostructure," *Optics Letters* 29, 1209-1211 (2004).
20. V. R. Almeida, Q. Xu, R. R. Panepucci, C. A. Barrios, and M. Lipson, "Light guiding in low index materials using high-index-contrast waveguides," in *MRS Proceedings*, (Cambridge Univ Press, 2003),
21. Q. Xu, V. R. Almeida, R. R. Panepucci, and M. Lipson, "Experimental demonstration of guiding and confining light in nanometer-size low-refractive-index material," *Optics Letters* 29, 1626-1628 (2004).
22. I. Khodadad, N. Clarke, M. Khorasaninejad, D. Henneke, and S. S. Saini, "Optimization of multiple-slot waveguides for biochemical sensing," *Appl. Opt.* 53, 5169-5178 (2014).
23. Q. Liu, X. Tu, K. W. Kim, J. S. Kee, Y. Shin, K. Han, Y.-J. Yoon, G.-Q. Lo, and M. K. Park, "Highly sensitive Mach-Zehnder interferometer biosensor based on silicon nitride slot waveguide," *Sensors and Actuators B: Chemical* 188, 681-688 (2013).
24. R. Sun, P. Dong, N. N. Feng, C. Y. Hong, J. Michel, M. Lipson, and L. Kimerling, "Horizontal single and multiple slot waveguides: optical transmission at $\lambda = 1550$ nm," *Opt. Express* 15, 17967-17972 (2007).
25. C. A. Barrios, Q. Xu, J. Shakya, C. Manolatu, and M. Lipson, "Compact silicon slot-waveguide disk resonator," in *Lasers and Electro-Optics, 2006 and 2006 Quantum Electronics and Laser Science Conference. CLEO/QELS 2006. Conference on*, (IEEE, 2006), 1-2.
26. C. A. Barrios and M. Lipson, "Electrically driven silicon resonant light emitting device based on slot-waveguide," *Opt. Express* 13, 10092-10101 (2005).
27. B. M. A. Rahman and J. B. Davies, "Finite-element solution of integrated optical waveguides," *Lightwave Technology, Journal of* 2, 682-688 (1984).
28. S. Elhadj, G. Singh, and R. F. Saraf, "Optical properties of an immobilized DNA monolayer from 255 to 700 nm," *Langmuir* 20, 5539-5543 (2004).
29. K. P. R. Nilsson and O. Inganäs, "Chip and solution detection of DNA hybridization using a luminescent zwitterionic polythiophene derivative," *Nature Materials* 2, 419-424 (2003).
30. N. Liu, M. Mesch, T. Weiss, M. Hentschel, and H. Giessen, "Infrared perfect absorber and its application as plasmonic sensor," *Nano Lett* 10, 2342-2348 (2010).
31. J. Xie, X. Jiang, Y. Zhong, Y. Lu, S. Wang, X. Wei, Y. Su, and Y. He, "Stem-loop DNA-assisted silicon nanowires-based biochemical sensors with ultra-high sensitivity, specificity, and multiplexing capability," *Nanoscale* 6, 9215-9222 (2014).
32. S. Golmohammadi and A. Ahmadvand, "Fano resonances in compositional clusters of aluminum nanodisks at the UV spectrum: a route to design efficient and precise biochemical sensors," *Plasmonics* 9, 1447-1456 (2014).
33. S. Boonruang and W. S. Mohammed, "Effect of the cladding layer on resonance response in guided mode resonance structures and its sensing applications," *JOSA B* 28, 671-678 (2011).

34. T. Claes, J. G. Molera, K. De Vos, E. Schacht, R. Baets, and P. Bienstman, "Label-free biosensing with a slot-waveguide-based ring resonator in silicon on insulator," *Photonics Journal, IEEE* 1, 197-204 (2009).
35. C. A. Barrios, K. B. Gylfason, B. Sánchez, A. Griol, H. Sohlström, M. Holgado, and R. Casquel, "Slot-waveguide biochemical sensor," *Optics letters* 32, 3080-3082 (2007).